MODELLING THE DYNAMICS OF THE SPACE DEBRIS ENVIRONMENT

A. Rossi

IFAC-CNR, Via Madonna del Piano 10, 50019 Sesto Fiorentino, Italy, Email: a.rossi@ifac.cnr.it

ABSTRACT

A full understanding of the dynamics of objects in the circumterrestrial environment is a fundamental step for the accurate modelling of the space debris population. Even more now, in a period of huge changes in the space traffic, with the continued accumulation of artificial objects around our planet and the plans of exploitation of new orbital regions. A short review of the main perturbative effects which are most important for the dynamics in different regions of the Earth orbit is given. Then the focus is moved to a review of some results obtained in the last years on the resonance effects in Earth orbit and on how these resonances could be exploited as transport mechanisms to remove spacecraft at the end-of-life. The analogies with the dynamics of the small bodies in the Solar System is shown to highlight the importance of the cross-fertilization between these two close-by research fields. Finally, some remarks are given on the collective behavior of large ensembles of objects by studying the dynamics of the cloud of fragments produced by in-orbit fragmentations. In particular, the complex evolution of the collision risk following a fragmentation of a satellite within a multi-plane constellation is discussed.

Keywords: Orbital dynamics, Solar System dynamics, Resonances, Fragmentations, Collective behaviors.

1. INTRODUCTION

In a period of huge changes in the space traffic and of continued accumulation of artificial objects around our planet, modeling the evolution of the debris environment has become even more important than ever. A fundamental step for the proper modeling of the debris population is the understanding of their dynamics in the Earth orbit and beyond.

Evolutionary models focused on different populations and different orbital regimes (e.g., LEO, MEO, GEO,...) can rely on specific dynamical settings, tailored to the accurate modeling of specific orbital perturbations, either gravitational or non-gravitational. Given the size of the simulated populations, the dynamical models must follow a trade off between accuracy and required CPU time, even if it is worth stressing that recent and future advances in computing power will help in this respect.

Specific examples and analogies with the dynamical evolution of the small bodies in our Solar System can help in understanding complex transport mechanisms within orbital regimes, allowing a fruitful cross-fertilization between the studies on the artificial and natural bodies populations.

Fragmentations, either explosion or collision-related, played a paramount role in the composition of the current debris environment. Despite the growing adoption of explosion prevention measures and of collision avoidance practices, the simulations show how fragmentations, and in particular accidental collisions, will continue to be a main source of debris in the future [29]. The outcome of such events represents a peculiar situation where the accurate modeling of the fragment clouds dynamical evolution can help in reducing the subsequent collision risk against other assets in nearby orbital regions.

It is worth stressing that the renewed interest in the exploration and exploitation of the Moon is quickly bringing to our natural satellite similar problems faced by the Earth orbital environment. The complex and chaotic dynamics in the cislunar space is the subject of many recent studies and is a blossoming field of research. The complete understanding of the dynamics in lunar orbits is of paramount importance for the appropriate management of the lunar orbit in view of its future massive exploitation. As an example of the pressing problems to be faced by the future lunar orbit traffic is the well known (in the Earth orbit case) issue of the disposal of spacecraft at the end-of-life, in the absence of an atmosphere and with the strong instability of the lunar orbits. The identification of viable disposal options requires a deep understanding of the dynamics in the cislunar space. This wide subject, albeit extremely important for the future space activities, is not the focus of this short review. The interested reader can refer to several contributions available also in this same volume.

2. ORBITAL PERTURBATIONS

A plethora of excellent text books on orbital dynamics exist (e.g., to name a few, [30], [8], [39], etc). It is not

Proc. 9th European Conference on Space Debris, Bonn, Germany, 1–4 April 2025, published by the ESA Space Debris Office
Editors: S. Lemmens, T. Flohrer & F. Schmitz, (http://conference.sdo.esoc.esa.int, April 2025)

doable, nor is the scope of this short paper, to provide extensive details on the orbital motion in Earth orbit. We just briefly mention the main effects that should be taken into account when trying to model the evolution of population of debris in the vicinity of our planet. In particular, we are interested in pointing out the main perturbative effects that are should be considered to have a realistic picture of the evolution on timescales ranging from

Fig. 1 shows the order of magnitude of the main accelerations affecting the orbits of objects around the Earth. Beyond the main effect, due to the monopole term of the Earth gravity potential, several other perturbations tend to alter the motion of an object with respect to a pure two body orbit. The atmospheric drag is the most important perturbation in LEO, since it subtracts energy from an orbiting object causing its decay into the atmosphere. It represents, therefore, the main sink process to be considered in the modeling. On the other hand, the atmosphere density is decreasing exponentially with the altitude, so that this perturbation is efficient only up to about 800 km above the surface of the Earth. As visible from Fig. 1, many other perturbations act on a satellite in LEO, but none of them causes a secular change in the semimajor axis.

Gravitational perturbations, due to the non-spherical shape of the Earth are important mainly in changing the angular arguments of the orbit (see Sec.4). The main effects of the geopotential perturbations are the secular regression of the orbital node, $\dot{\Omega}$ and the precession of the perigee argument ($\dot{\omega}$). Most of the effect is related to J_2, the quadrupole term of the gravity potential expansion in terms of spherical harmonics ([16]), due to the Earth oblateness.

With growing distance from the center of the Earth, different perturbations become important. While the main effects are still due to the J_2 term, the gravitational perturbations due to the differential attraction of Sun and the Moon, become comparable. The lunisolar attraction induce long-term and sometimes secular variations in the eccentricity, inclination, argument of the node and of perigee. As a matter of fact, lunisolar perturbation, coupled with air drag, may play a role in speeding the orbital decay of certain classes of highly eccentric orbits, by lowering the perigee height ([11]).

At higher altitudes, another non-gravitational perturbation starts to play a rôle: the solar radiation pressure (SRP) (e.g., [18]). For objects with area to mass ratios in the range 0.01 to 0.1, typical of orbiting spacecraft, its effect is mainly a long periodic (i.e. approximately yearly) change of the orbital eccentricity and of the argument of perigee. For larger area to mass ratios, e.g. spacecraft with where large antennas or panels, it can lead to even higher accelerations w.r.t. those depicted in Fig. 1. More complex effects, leading to long term perturbations on the semimajor axis, inclination and node, can be caused by the effect of the radiation pressure on the spacecraft antenna ([18]). Even more pronounced effects are visible in the dynamics of the so-called "high are-to-mass ratio"

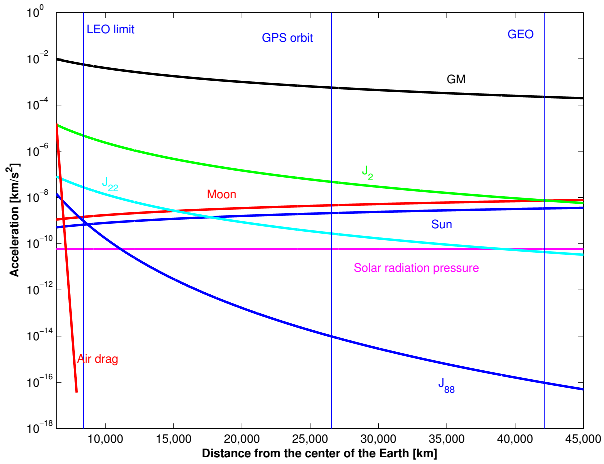

Figure 1. Order of magnitude of different perturbations affecting the orbit of an Earth satellite. The area over mass ratio assumed for the calculation of the air drag and solar radiation pressure accelerations is $A/M = 0.01$ m^2 kg^{-1}. The air drag acceleration is computed considering a simple exponential model for the atmospheric density. The vertical lines mark the altitude of 2000 km above the Earth surface, the altitude of the GPS orbit and the Geostationary radius.

(A/M) objects identified in telescopic observation in the early 2000's ([34], [33]). For these very peculiar objects, with A/M in excess of 10 m^2/kg, the SRP induces a very long term, or even secular, increase of e and i leading them from their original GEO orbit to high eccentric and inclined ones, keeping their mean motion (i.e., orbital energy) $n \approx 1$ ([17], [38]). Whereas not particularly important in terms of their environmental effects in a big modeling effort of the whole debris population, the dynamics of these peculiar objects reminds us of the importance of a full understanding of the effects of a given perturbation whenever the "usual" assumptions are not valid any more.

Looking at Fig. 1 it can be noticed how in the GEO region, at more than six Earth radii, the balance of the accelerations acting on a spacecraft change considerably and the third body effects become comparable to those due the Earth oblateness. Together they cause a precessional motion of the orbital plane, inducing the oscillation with a period of ≈ 53 years around the stable Laplace plane at $i \approx 7.2°$ (e.g., [4], [12], [21]), that reflects in the known wave-like distribution of the equatorial inclinations of the abandoned GEO objects [35].

In reality the picture of the perturbations acting on an Earth satellite is more complex than what is depicted in Fig. 1. As an example, different kinds of resonances between the motion of the orbiting object, the rotation of the Earth and the motion of the perturbing bodies can produce long term and even secular perturbations exceeding those due to the simple action of a given perturbation alone (e.g., [16], [13], [6]). This is the subject of the next Section.

3. RESONANCES

From a dynamical point of view, the most well-known resonances in Earth orbit are the so-called mean motion resonances (MMR). From an analytical point of view, these resonances can be studied by means of the Kaula's theory of satellite motion ([16], [13]). In MMRs, the exact condition for commensurability is that the satellite performs β nodal periods while the Earth rotates α times relative to the precessing satellite orbit plane, where α and β are mutually prime integers. In the case of GEO we have $\alpha = \beta = 1$, while for MEO GNSS-like orbits, whose orbital period equals about half a sidereal day, $\alpha = 1$ and $\beta = 2$. After this interval the path of the satellite relative to the Earth repeats exactly leading to the resonance. The approximate condition is that the mean motion of the satellite is β/α times the angular velocity of the Earth. Note that while the deep resonances are not always met in the satellite orbits, *shallow resonances* still yields substantial perturbations and are common features.

Geostationary satellites are resonant with the coefficients of the Earth's gravity field with low degree and even values of the difference between the order ℓ and the degree m of the coefficients $(\ell - m)$, in particular the J_{22} term related to the ellipticity of the Earth's equator [16]. This resonance causes the satellite's longitude to librate with a very long period (of the order of 1000 days) about two stable equilibrium positions, located at the longitude of $75°$ East and $245.5°$ East (two unstable equilibrium points are located at $161.8°$ and $348.5°$ E). The 2:1 resonance causes long period changes in the orbital eccentricity of MEO satellites and, for example, can modify the configuration of the navigation constellations.

A more complex resonance, resulting from the third body and the geopotential perturbations, is the cause of a very long term-term (nearly secular) perturbation of the eccentricity of the navigation satellites orbits, representing a serious hazard for the long term disposal of the spent satellites and upper stages in the region ([6], [27]). This luni-solar resonance appears when the secular motions of the lines of apsides and nodes become commensurable with the mean motion of the Sun and the Moon ([14]).

As mentioned above, the resonances can destabilize a dynamical system. As such, they can be seen as a nuisance for the type of ordered motion required in a satellite system, such as a constellation. On the other hand, orbital resonances can also be exploited as a mean to transport objects within a system.

This consideration stems from the analogy with the dynamics of our Solar System (SS). As it is well known (e.g., [5] and references therein) the mean motion and secular resonances (where orbital frequencies are commensurate with the solar system's natural frequencies) are sculpting the geography of the main asteroid belt (MB) and are responsible for the transport of some of the smallest objects from the MB to the inner SS where they become Near Earth Asteroids (NEA). Asteroid fragments, generated by collisions in the MB are directly in-

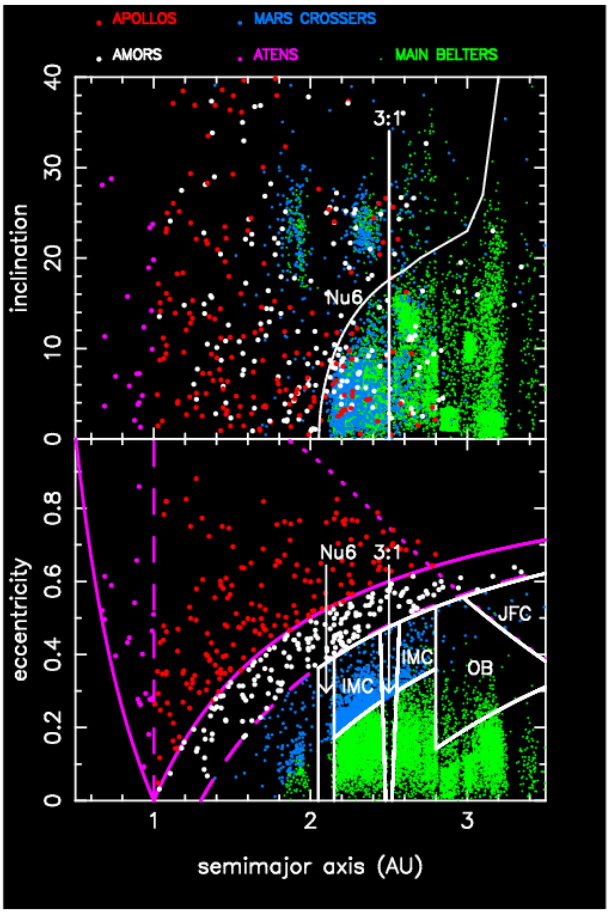

Figure 2. Orbital distribution of main belt asteroids (green), Intermediate Mars Crossers (blue) and NEOs (white, red and magenta) (Image from: A. Morbidelli et al., Understanding the distribution of NEAs).

jected or slowly moved via Yarkovsky thermal drag [10] into both MMR with the planets and secular resonances. The main resonances responsible for the transport of the NEAs are the 3 :1 MMR with Jupiter (white vertical line in the top panel of Fig. 2) and the ν_6 secular resonance, defined by the relation $g \sim g_6$, where g is the rate of precession of the longitude of pericenter of an asteroid and g_6 is the sixth eigenfrequency of the solar system planets (approximately the rate of precession of Saturn's longitude of pericenter) (curved white line in the top panel of Fig. 2). Other minor contributions come from the 5:2 MMR resonance with Jupiter. The eccentricities (and inclinations) of the asteroids are modified by the resonant perturbations and/or by planetary encounters until they reach the NEA region, in the inner SS. Last, but not least, it has to be noted that the web of resonances, and their overlapping, is responsible for the onset of the well know chaotic behavior in the motion of the asteroidal population [7], [19].

An analogous web of resonances, involving Earth gravity potential, third body and SRP perturbations, along with overlaps and chaotic regions, can be identified in the circumterrestrial region. A long stream of papers was devoted, in recent years, to the characterization of this complex web of resonances and the interested reader is invited to see those papers (see e.g., [9], [22], [1], [2], [3], [22], [32], [36], [23] and references therein). Here we will only recall a few of the main results of those researches. One of the purpose of the above listed studies was to identify, again in analogy with the SS, transport routes to speed up the de-orbiting of the spacecraft at the end of life. This aim could be achieved by moving, whenever possible, the spacecraft within a nearby resonance region where its eccentricity will be pumped up leading it toward an accelerated reentry into the atmosphere. In this respect, a paramount rôle can be played by resonances including the SRP. For these reason, the use of small solar sails, to be deployed at the end-of-life, can by hypothesized to increase the A/M augmenting the effectiveness of the SRP effect. For this purpose a thorough theoretical analysis and an extensive numerical investigation were performed.

The eccentricity variations occur mainly in correspondence of the resonances defined by the following relation:

$$\dot{\psi} = \alpha\dot{\Omega} \pm \beta\dot{\omega} \pm \gamma n_s \simeq 0 \qquad (1)$$

where n_s is the apparent mean motion of the Sun with respect to the ecliptic plane. α, β, $\gamma = 0, \pm 1, \pm 2$ depending on the perturbation. From Eq. 1, Tab. 1 lists the main resonances found in the LEO environment.

These resonances cause an increase in the orbital eccentricity and, as such, can be viewed as "de-orbiting corridors". An object placed in one of these "corridors" can get its eccentricity increased secularly until it reaches the atmosphere, at perigee, leading to a reduced lifetime (see, [28] for details). The perturbative effect can be explained by computing the equilibrium points and the stability of the dynamical system associated with solar radiation pressure and Earth's oblateness. The natural deorbiting can occur in two situations, either by following the hyperbolic invariant curves stemming from a saddle equilibrium point or by following a wide enough libration curve in the neighborhood of an elliptic equilibrium point. The initial condition for the de-orbiting corridors can be computed as a resonant condition involving the rate of precession of Ω, ω and the apparent mean motion of the Sun with respect to the ecliptic plane (n_s). Figure 4 shows the location of the main MEO and LEO resonances for enhanced $A/M \sim 1$ m^2 kg^{-1}, following the classification of Tab. 1. Following the idea of the resonant deorbiting corridors, Fig. 4 shows again the location of the resonances in the inclination-semimajor axis space superimposed on a color map showing the residual lifetime, as a function of the initial inclination and semi-major axis, computed in 120 years for an object with $A/m = 1$ m^2 kg^{-1}, starting from $e = 0.001$, $\Omega = 0°$ and $\omega = 0°$. The red dots show the location of the spacecraft according to the spacecraft in the catalogue at the time of the simulation.

By means of dedicated long term simulations of the whole debris population, performed with a dedicated branch of the SDM model [26], it has been shown how the de-orbiting corridors could be very effective in removing the objects from the high LEO region at the end-of-life, thus contributing to the stabilization of the space debris environment, in particular for high-altitude spacecraft.

Argument ψ_j	α	β	γ	Index j
$\Omega + \omega - \lambda_S$	1	-1	1	1
$\Omega - \omega - \lambda_S$	1	-1	-1	2
$\omega - \lambda_S$	0	1	-1	3
$\omega + \lambda_S$	0	1	1	4
$\Omega + \omega + \lambda_S$	1	1	1	5
$\Omega - \omega + \lambda_S$	1	-1	1	6
$\Omega + 2\omega - 2\lambda_S$	1	2	-2	7
$2\Omega + 2\omega - 2\lambda_S$	2	2	-2	8
ω	0	1	0	9
$\Omega + 2\omega$	1	2	0	10
$2\Omega + 2\omega$	2	2	0	11

Table 1. List of the main resonances expected to be found in LEO: argument ψ_j , values of the coefficients α, β, γ and corresponding index j. Resonances from $j = 1$ to $j = 6$ are due to the SRP; resonances 7 and 8 are singly averaged Solar gravitational resonances; resonances from 9 to 11 are doubly averaged lunisolar resonances (see [32])

Furthering the analogy with the SS dynamics, it is interesting to note that resonances similar to those identified above for the Earth orbits, are also deemed responsible for the chaotic dynamics in the "inert Oort cloud" (IOC), defined as the transition region between the outer Kuiper belt and the Oort cloud, where planetary perturbations and galactic tides share the same order of magnitude. The IOC spans between ≈ 500 and 1600 au, or more precisely, a region where the semi-major axis is smaller than 1600 au and the perihelion distance is larger than 45 au, but the semi-major axis should be larger than 500 au if the perihelion distance is smaller than 80 au. [31]. The zone is scarcely populated and a few bodies have been discovered within this region: (90377) Sedna, 2012 VP$_{113}$ and 2015 TG$_{387}$ (see [31] and references therein).

It turns out that the problem is formally close to the case of a satellite perturbed by the J_2 flattening of the Earth and the averaged attraction from the Sun. The Hamiltonian for the averaged quadrupolar effect of inner bodies has the same form as a J_2 flattening of the central body (see e.g. [37]). On the other hand, the galactic tides act similarly to the third body perturbations (and/or SRP) in the satellite case. As such, the system possesses a tilted Laplace plane (the "galactic Laplace plane"), with a crossover located at about 1000 au. For semi-major axes much smaller than this value ($\sim$ 500 au), circular orbits precess about the ecliptic pole, whereas for semi-major axes much larger than this value (~ 1500 au) they precess about the galactic pole. In between, they precess about an intermediately tilted pole [31]. Moreover, it can be shown that in the IOC the precession velocities of Ω and ω with respect to the ecliptic inclination I, follow the same rules as for an Earth satellite. I.e., ω increases for $I < 63°$, decreases for $63° < I < 117°$, and increases again for

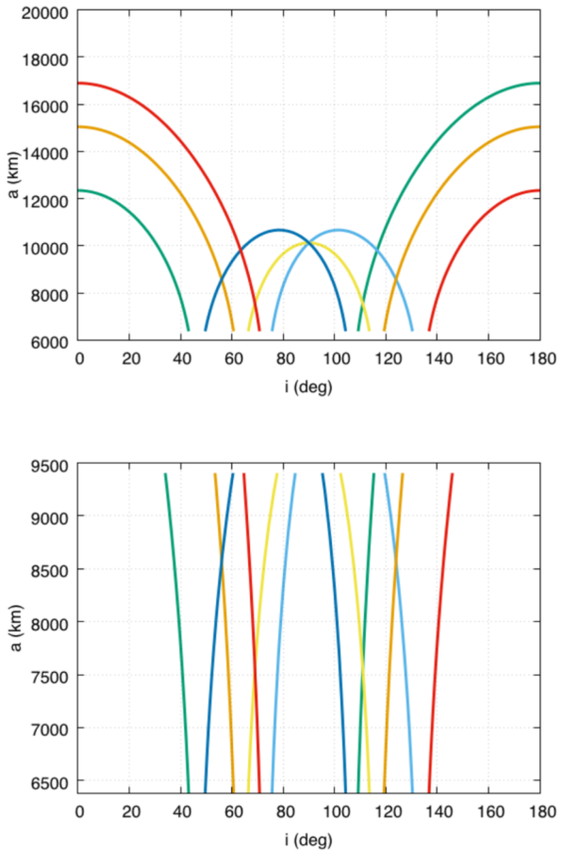

Figure 3. On the top, we show the location of the six main SRP resonances (Tab. 1) as a function of i, a for $e = 0.01$. On the bottom, a close-up in the LEO region, defined here up to $h = 3000$ km, in order to account also for possible graveyard orbits. The curves were computed assuming $\dot{\Omega} = \dot{\Omega}_{J2}$ and $\dot{\omega} = \dot{\omega}_{J2}$. Green: $\dot{\Omega} + \dot{\omega} - n_S = 0$. Cyan: $\dot{\Omega} - \dot{\omega} - n_S = 0$. Orange: $\dot{\omega} - n_S = 0$. Yellow: $\dot{\omega} + n_S = 0$. Blue: $\dot{\Omega} + \dot{\omega} + n_S = 0$. Red: $\dot{\Omega} - \dot{\omega} + n_S = 0$. From: [2].

$I > 117°$, while Ω decreases for $I < 90°$ and increases for $I > 90°$. Just as was shown in the Earth case, the precession angles are coupled in integer combination which, through the galactic tide effect, vanish in correspondence of specific resonances. Figure 5 shows a map of these precession velocities with respect to the ecliptic inclination, as well as the places where their main integer combinations vanish. It is worth noting how the $k\omega + j\Omega$ combinations listed in the figure corresponds to those listed in Tab. 1 for the Earth case, showing the power of the analytic theory developed for the analysis of these complex resonance problems and the nice interchanges of knowledge and competences linking spaceflight dynamics and celestial mechanics.

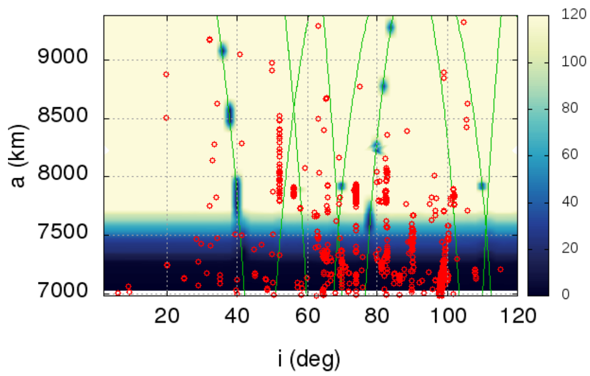

Figure 4. Location of the resonances in the inclination-semimajor axis space. The color bar shows the residual lifetime, in years, for an object, with an augmented $A/M \sim 1$ m^2 kg^{-1}, left in a circular orbit of the given point of the phase space. The blue islands along the main resonances, warranting a lower residual lifetime, can be noticed. The population of spacecraft in the catalogue at the time of the simulation is superimposed as red circles.

4. COLLECTIVE BEHAVIORS: IN-ORBIT FRAGMENTATIONS

As mentioned in Sec. 1, fragmentations, represent the main source of debris in the current debris environment. The long term modeling is telling us that fragmentations, and in particular accidental collisions, will continue to be a main source of debris in the future (e.g., [29]). Many studies devoted to the dynamics of the debris clouds produced by a fragmentation can be found in the literature. The dynamics of a fragmentation cloud produces collective behaviors (that can also be analyzed with different techniques, akin to the fluid and statistical mechanics) that have to be considered to understand and, possibly minimize, the consequences for the other orbiting assets in the same region of space. In an extreme synthesis, we can summarize the well known generation of the cloud starting with an initial energetic ejection of the fragments from the location of the parent object, usually modeled (e.g., in the NASA standard breakup model, [15]) as isotropic. The ΔV imparted to the fragments pushes them into orbits different from the original one (in particular in terms of a and e) with different evolutionary paths. This leads quickly to the creation of the toroidal structure around the parent object's orbit. The timescale of this process can be easily estimated by considering the synodical period, S, of the fragments w.r.t. the one of the fragmented object:

$$\frac{1}{S} = \frac{1}{k}\left(\frac{1}{a_{\text{frag}}^{3/2}} - \frac{1}{a_{\text{parent}}^{3/2}}\right) \tag{2}$$

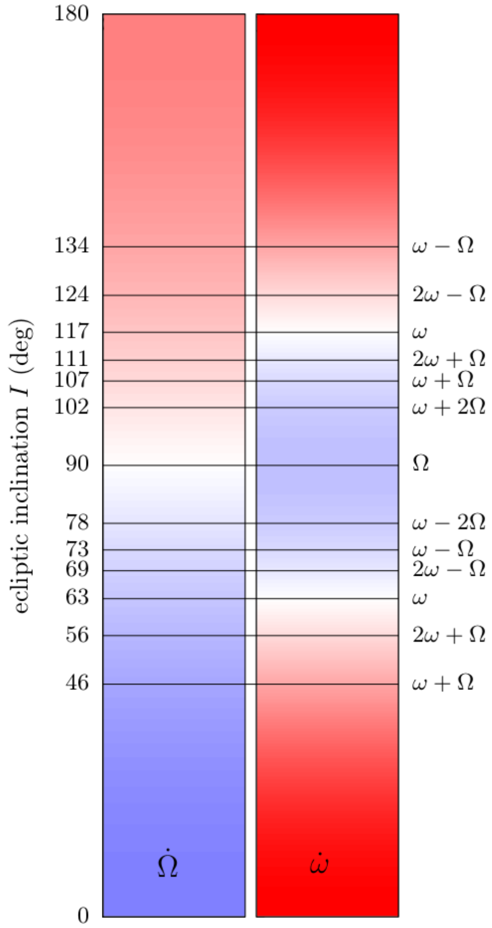

Figure 5. Precession velocity of Ω and ω in the planetary regime. The color represents the velocity scale from negative values in blue to positive values in red, with the same color scale for both angles. The locations where the integer combinations $k\dot{\omega} + j\dot{\Omega}$ vanish (limited to $||k||, ||j|| < 3$) are shown by horizontal lines. The inclination values listed on the left correspond to the constant angles combination written on the right.(Image from: [31]).

where $k = \frac{2\pi}{\sqrt{GM}}$ and a_{frag} and a_{parent} are the semimajor axis of the fragment and of the parent object, respectively. Considering a cloud generated by typical spacecraft or rocket bodies fragmentations in highly inclined ($\sim$ 80°) LEOs, at about 800 km of altitude, the 70^{th} percentile of the fragments' S, can be considered a reliable estimation of the formation time of the torus. This value ranges from $\sim$ 6 to $\sim$ 14 days (corresponding to $\sim$ 75 and $\sim$ 235 revolution of the parent object, respectively). Note that the typical S periods for fragmentation in Highly Elliptical Orbits (HEOs), such as the Molniya ones, are $\sim$ 3 times longer in terms of days (while comparable if considered in units of the parent object orbital period).

Further on in the evolution, the effect of the flattening of the Earth (parametrized by the J_2 coefficient in the spherical harmonics expansion of the geopotential, e.g., [30]) spreads the nodes of the fragments' orbits, leading to the creation of a shell of fragments around the altitude of the event (note that the J_2 effect is also contributing to the torus formation through the randomization of the arguments of perigee). Again the timescale for the formation of the shell can be estimated simply by computing the synodical period of the nodal precession of the fragments w.r.t. the one of the fragmented object: $\frac{1}{S_\Omega} = \frac{1}{T_{\Omega_{\text{frag}}}} - \frac{1}{T_{\Omega_{\text{parent}}}}$, where $T_{\Omega_{\text{frag}}}$ and $T_{\Omega_{\text{parent}}}$ are the periods of the precessing node of the fragment and of the parent object's orbit, respectively. It can be assumed that the shell formation is reasonably completed once a given percentage (e.g., 70 %) of the fragments have their node 180° apart from the precessing parent object, i.e., after half the full synodic period of the precession. The argument of perigee randomization can be estimated with the same methodology. The timescale of the Ω randomization, for a typical fragmentation in highly inclined ($\sim$ 80°) LEOs, at about 800 km of altitude, is about $300 \div 350$ days (corresponding to $\sim$ 5000 orbital periods of the parent object). The timescale for a similar event in HEOs (specifically Molniya orbits) is about 8 times longer due to the reduced J_2 effect, owing to the larger distance. The timescale for the ω randomization in LEO is about half than the one for the argument of the node. Of course, being related to the J_2 effect, the timescale of the Ω and ω randomization is strongly dependent on the orbital inclination of the parent object [30].

The proper evaluation of the timescales of the cloud evolution is particularly important to asses the effects and the risks posed by a fragmentation on other assets orbiting in nearby regions of space. In particular, when a fragmentation happens within a large ordered ensemble of satellites, such a Walker-type constellation, the above described cloud evolution can lead to interesting collective behaviors, that were analyzed first in [24], that could enhance the impact risk. The architecture of a multi-plane constellation can make a break-up event particularly dangerous, owing to the above described spreading of the resulting fragment swarms. This is particularly true when differential precession of the orbits leads the fragments to encounter satellites revolving around the Earth in the opposite direction (Fig.6). This makes head-on collisions possible, despite the almost equal equatorial inclination of the fragments and the constellation satellites, with higher impact speeds and greater collision probability. The coupled dynamics of the cloud and the constellation planes and the corresponding flux of projectile impinging against a spacecraft can be conveniently modelled by applying Öpik's [20] expression for the intrinsic collision probability p per unit of time for a pair of orbiting bodies. Öpik's theory, once again mediated from the studies on the SS dynamics, allows the computation of the collision probability in such a complex configuration by a simple analytical formula based on the orbital elements of the target (on a circular orbit) and of any pro-

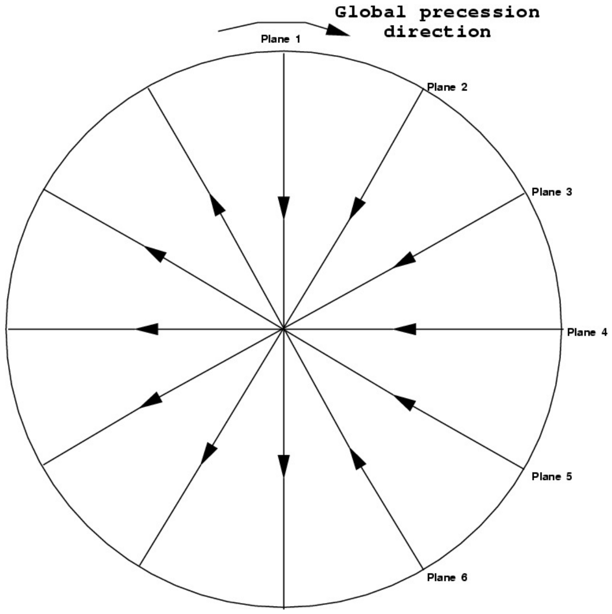

Figure 6. The orientation of the six orbital planes of an Iridium—like constellation, as seen from the celestial north pole. The revolution of the satellites is indicated by the arrows. Note the "counter—rotating" planes 1 and 6. If a satellite orbiting in either of these planes is disrupted, its fragments will pose an impact hazard higher than average to the satellites in the other plane. (Picture taken from: [24].

jectile crossing its orbit, as:

$$P = \frac{U}{2\pi^2 a^{1.5} |U_x| \sin I} \tag{3}$$

where a is the semimajor axis of the projectile, I is the relative inclination between the orbits of the projectile and the target, and U and U_x are, respectively, the projectile velocity relative to the target, in units of the target's geocentric velocity, and its component along the radial direction. It turns out that the relative dynamics of the constellation spacecraft in the precessing orbital planes and of the dispersing cloud of fragments leads to "waves" of increased particle flux (significantly higher than the background one) against the different precessing orbital planes, as time goes by, with different magnitude of the effects and timescales according to the initial plane of the fragmentation event (see [24], [25] for details).

Clearly nowadays, with the efficient collision avoidance procedures in effect, most of the potential collisions against trackable fragments could be avoided. Nonetheless, the number of Lethal Non Trackable particles produced by a fragmentation can be very high, still leading to a transient period of increased risk after an event. Therefore the proper understanding of the dynamics of a debris cloud, its intrinsic timescales and its subsequent interaction with the nearby orbiting assets remains of paramount importance.

ACKNOWLEDGMENTS

The author wishes to acknowledge funding from the Italian Space Agency (ASI Contract "Detriti Spaziali - Supporto alle attività IADC e SST 2023-2025"). Part of the work described in the paper was done under the Horizon 2020 Program of the European Union Framework Program for Research and Innovation (H2020-PROTEC-2015) under REA grant agreement n. [687500] - ReDSHIFT.

REFERENCES

1. Alessi, E.M., Schettino, G., Rossi, A., Valsecchi, G.B., (2018). Natural highways for end-of-life solutions in the LEO region, *Celest. Mech. Dyn. Astron.*. 130, 34.
2. Alessi, E.M., Schettino, G., Rossi, A., Valsecchi, G.B., (2018). Solar radiation pressure resonances in Low Earth Orbits, *Mon. Not. R. Astron. Soc.*, 473, 2407–2414.
3. Alessi, E.M., Colombo C. and Rossi, A., (2019). Phase space description of the dynamics due to the coupled effect of the planetary oblateness and the solar radiation pressure perturbations, *Celest. Mech. Dyn. Astron.*, 131:43.
4. Allan, R.R. and Cook, G.E., (1964). The long-period motion of the plane of a distant circular orbit, *Proc. R. Soc. Lond. A*, 280, 97-109.
5. Bottke W.F., Jr., Jedicke R., Morbidelli A., Petit J-M, and Gladman B., (2000). Understanding the Distribution of Near-Earth Asteroids, *Science*, 288, 5474, pp. 2190-2194, DOI: 10.1126/science.288.5474.219.
6. Chao G., Hoots F., (2019). *Applied Orbit Perturbation and Maintenance, Second Edition*, Aerospace Press.
7. Chirikov, B.V., (1979). A universal instability of many-dimensional oscillator systems. *Phys. Rep.*, 52, 263–379.
8. Chobotov A.V., (2002) *Orbital Mechanics, Third Edition* ISBN (print): 978-1-56347-537-5, eIS.BN: 978-1-60086-225-0, AIAA Education Series.
9. Daquin , Rosengren A.J, Alessi E.M., Deleflie F., Valsecchi G.B. and Rossi A., (2016). The dynamical structure of the MEO region: long-term stability, chaos, and transport, *Celest. Mech. Dyn. Astr.*, 124:335–366.
10. Farinella P. and Vokrouhlický D., (1999). Semimajor Axis Mobility of Asteroidal Fragments, *Science*, 283, 5407, 1507-1510, DOI: 10.1126/science.283.5407.1507
11. Frazier W., Culp R.D. and Rosborough G., Semianalytical study of high-eccentricity orbit evolution, *Astrodynamics 1989* 1990, 71 Part II, Univelt Incorporated, San Diego, CA, USA, 1251–1264.
12. Friesen, L.J., Jackson, A.A., Zook, H.A. and Kessler, D.J., (1992). Analysis of Orbital Perturbations Acting on Objects in Orbits Near Geosynchronous Earth Orbit, *J. Geophys. Res.*, Vol. 97, 3845-3863.

13. Gedeon G.S., (1969). Tesseral resonance effects on satellite orbits, *Cel. Mech. Dyn. Astr.*, 1, 167–189.

14. Hughes S., (1980). Earth satellite orbits with resonant lunisolar perturbations. I. Resonances dependent only on inclination, *Proc. R. Soc. Lond. A.*, 372: 243–264.

15. Johnson N.L., et al., (2021). NASA's new breakup model of evolve 4.0. *Advances in Space Research*, 28, 1377–1384.

16. Kaula W.M, (2000) *Theory of Satellite Geodesy*. Blaisdell (Dover, November 2000)

17. Liou, J.-C., Weaver, J. K., (2005). Orbital dynamics of high area-to-mass ratio debris and their distribution in the geosynchronous region. In: Danesy, D. (Ed.), *Proceedings of the Fourth European Conference on Space Debris* (ESA SP-589). ESA Publications Division, Noordwijk, The Netherlands, pp. 285–290.

18. Milani A., Nobili A. and Farinella P., (1987) *Non gravitational perturbations and satellite geodesy*, Adam Hilger Ltd., Bristol and Boston.

19. Morbidelli A., (2002). *Modern Celestial Mechanics: Aspects of Solar System Dynamics*, Taylor & Francis, London.

20. Öpik, E.J., (1976). *Interplanetary Encounters*. Elsevier, New York

21. Rosengren A.J., Scheeres D.J., and McMahon J.W., (2013). The Classical Laplace Plane and its use as a Stable Disposal Orbit for GEO 26^{th} *AMOS Conference*, Maui, Hawaii, USA.

22. Rosengren, A.J., Alessi, E.M., Rossi, A., Valsecchi, G.B., (2015). Chaos in navigation satellite orbits caused by the perturbed motion of the Moon. *Mon. Not. R. Astron. Soc.*, 449, 3522–3526.

23. Rosengren, A.J., Skoulidou, D.K., Tsiganis, K. and Voyatzis G., (2019). Dynamical cartography of Earth satellite orbits, *Adv. Spa. Res.*, 63, 1, 443-460. https://doi.org/10.1016/j.asr.2018.09.004

24. Rossi A., Valsecchi G.B. and Farinella P., (1999). Risk of collision for constellation satellites, *Nature*, 399: 743–744.

25. Rossi A., Valsecchi G.B. and Farinella P., (2000). Collision risk for high inclination satellite constellations *Planetary and Space Science*, 48, 319 - 330.

26. Rossi A., L. Anselmo, C. Pardini, G.B. Valsecchi, R. Jehn, (2009). The new space debris mitigation (SDM 4.0) long-term evolution code, *Proceedings of the 5^{th} European Conference on Space Debris*, SP-672, Darmstadt, Germany.

27. Rossi A., (2008). Resonant dynamics of Medium Earth Orbits: space debris issues. *Celest. Mech. Dyn. Astr.*, 100: 267-286.

28. Rossi A., Alessi, E.M., Schettino, Valsecchi, G.B., Schaus V., (2020). How an aware usage of the long-term dynamics can improve the long-term situation in the LEO region, *Acta Astronautica*, 174, 159–165.

29. Rossi et al., (2023). Long term effects of the mitigation and remediation measures in view of the changing space activities, *The Second International Orbital Debris Conference*, December 4-7, 2023, Sugar Land, Texas, USA.

30. Roy A.E., (2004). *Orbital motion (4th ed.)*, Taylor and Francis, eBook ISBN 9780367806620.

31. Saillenfest M., Fouchard M., Ito T. and Higuchi A., (2019). Chaos in the inert Oort cloud, *A&A*, 629, A95, DOI: 10.1051/0004-6361/201936298 .

32. Schettino G., Alessi E.M., Rossi A., Valsecchi G.B., (2019), A frequency portrait of Low Earth Orbits, *Celest. Mech. Dyn. Astr.*, 131:35.

33. Schildknecht, T., Musci, R., Ploner, M., et al., (2004). Optical observations of space debris in GEO and in highly-eccentric orbits. *Advances in Space Research*, 34, 901–911.

34. Schildknecht, T., Musci, R., Flury, W., et al., (2005). Optical observations of space debris in high-altitude orbits. In: Danesy, D. (Ed.), *Proceedings of the Fourth European Conference on Space Debris*, ESA SP-587. ESA Publications Division, Noordwijk, The Netherlands, pp. 113–118.

35. Schildknecht, T., (2007). Optical surveys for space debris, *Astron. Astrophys. Rev.*, 14, 41-111.

36. Skoulidou, D.K., Rosengren, A.J., Tsiganis, K. and Voyatzis G., (2018). Dynamical lifetime survey of geostationary transfer orbits. *Celest. Mech. Dyn. Astr.*, 130, 77. https://doi.org/10.1007/s10569-018-9865-1

37. Tremaine, S., Touma, J., & Namouni, F., (2009). Satellite dynamics on the Laplace surface, *AJ*, 137, 3706.

38. Valk, S., Lemaître, A., Anselmo, L., (2008). Analytical and semi-analytical investigations of geosynchronous space debris with high area-to-mass ratios influenced by solar radiation pressure, *Advances in Space Research* 41, 1077–1090.

39. Vallado D., McCain W., (2001) *Fundmentals of Astrodynamics and Applications*, Microcosm Press, El Segundo, CA